Phase-Delay Rabi-Flopping Spectroscopy: A Method Sensitive to Rydberg Species at Surfaces

Leif Holmlid[§]

Atmospheric Science, Department of Chemistry, Göteborg University, SE-412 96 Göteborg, Sweden

Received: August 17, 2004; In Final Form: September 27, 2004

Spectra observed with grating spectrometers from surface layers on alkali-promoted catalysts are studied with a confocal microscope setup, focusing to a nominal resolution of a few micrometers. The spectra are quite similar to Raman spectra but are caused by phase-delayed light with no wavelength shift. Strong effects related to circularly polarized light are observed, supporting the phase-delay process. That information from the surface layer is obtained is proved since the spectra vary over the emitter surface and with the microscope distance to the surface. The theory for phase-delay spectroscopy is developed. In the anti-Stokes range, the spectral shifts correspond to energy differences between levels connected by forbidden transitions, for example, between a high Rydberg level and the ground state in the K atom. Transitions mediated by Rydberg species are instead observed in adsorbed molecules in the Stokes range.

1. Introduction

Raman-like spectra can be observed at surfaces where Rydberg species are formed in desorption; however, shifts of frequency observed with grating spectrometers are only apparent since the frequency of light is not shifted even if the position in the spectrum seems to indicate this. In a recent micro-Raman study[1] of the K* $-H_2O$ Rydberg complex on a heterogeneous catalyst surface, we observed several non-Raman bands that could still be identified by changing the sample conditions such as surface temperature and gas inlet. We proceed now to identify the mechanisms behind this type of spectrum. This may mean that a new method for spectroscopy of surfaces, and especially of catalyst surfaces under operating conditions, will become available.

The importance of Rydberg states at catalyst surfaces is coupled to their large reactivity, which is caused both by the very large cross sections for collisions and the excess energy available in the Rydberg states. The formation of excited complexes such as K* $-H_2O$[1] or K* $-N_2$ (proposed for the ammonia catalyst[2]) will strongly influence the reactivity on the catalyst surface. Many alkali-promoted heterogeneous catalysts are used at relatively high temperatures, and the thermal formation of Rydberg states of the alkali atoms has been studied with different methods for quite some time. For example, the desorption of Rydberg species from various alkali-promoted catalysts is studied by Kotarba et al.[3−5] They even observe that catalytically active surfaces emit Rydberg species, while similar, catalytically inactive or "poisoned" surfaces do not give Rydberg species formation. The formation of Rydberg clusters of alkali atoms desorbing from similar surfaces is investigated by molecular beam methods in a few studies.[6−8] That Rydberg species are formed thermally is also demonstrated clearly since a thermal laser, the Rydberg Matter laser, is shown to operate, albeit so far only at low intensities.[9,10]

It is obvious that Raman scattering in general will be a very useful method to study long-lived Rydberg species. Other similar processes involving two photons also have good potential for studies of Rydberg species. In some recently published Raman techniques, the Raman scattering may involve Rydberg states.[11,12] The reason for the usefulness of Raman and similar techniques is the extremely large polarizability of circular Rydberg species, of the order of 10^9 times larger than for ground state atoms. As mentioned above, Raman scattering is indeed observed in systems with long-lived Rydberg species. Due to the extreme polarizability, it is likely that effects will be seen that otherwise are only observed with extremely large laser intensities for systems with small values of polarizability. In the present contribution, it is concluded that such processes in the form of Rabi flopping are observed with a CW laser.

In fact, the Rydberg species act as antennas, coupling the laser light into the neighboring molecules or Rydberg complexes containing the molecules. This means that a strong relation exists between the presently described phase-delay method and surface-enhanced Raman scattering (SERS):[13−15] instead of antenna particles with a size smaller than the wavelength of the light as in SERS (often of the order of 100 nm), the Rydberg species have a similar size and couple strongly to the light field due to their large polarizability. The enhancement in SERS is considered to be 10^3-10^{12} relative to Raman scattering, and the enhancement due to the Rydberg species may be of the order of 10^9, based on the size of their polarizability.

We describe here the first systematic study of a phase-delay spectroscopic method useful for the study of Rydberg species. This method uses a phase shift due to a type of Rabi-flopping process. In this case, the photons from the laser are delayed in the Rydberg atom or complex, the delay given by the Rabi-flopping frequency far off resonance. The spectra observed with the spectrometer resemble anti-Stokes and Stokes Raman spectra. One interesting fundamental aspect of this method is that the excitation state of the scatterer is observed while the state does not change.

2. Theory

2.1. Flopping Quasitransitions. The probability of photon scattering from atoms and molecules is proportional to the

§ E-mail: holmlid@chem.gu.se.

10.1021/jp046288m CCC: $27.50
Published on Web 12/01/2004

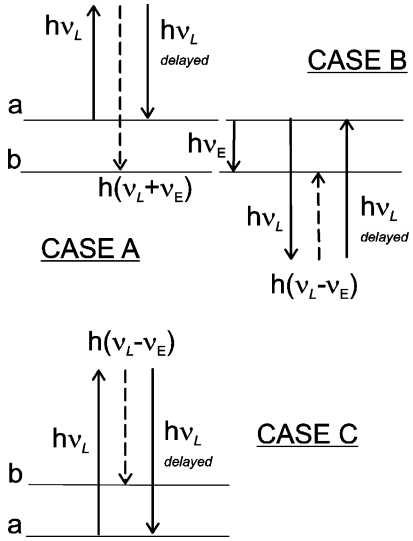

Figure 1. Energy diagram for the off-resonance Rabi-flopping process. The absorbed photon leaves the scattering system with a delay that is determined by the energy for the more or less forbidden transfer to the *b* state, which is often the ground state.

polarizability tensor with elements α_{ij}. The polarizability of an atom is approximately proportional to the volume of the atom, which means that a Rydberg state has a very high polarizability. For circular Rydberg states, the polarizability varies as n,[7] where n is the principal quantum number.[16] Thus, a high circular Rydberg state with $n = 100$ has a polarizability 6×10^9 times larger than the lowest Rydberg state for K, the 4f state, and even much larger than a ground-state H atom.

Due to the very strong scattering interaction between light and Rydberg species, this interaction is best described in the form normally used for the interaction of very intense lasers with matter.[17] An energy diagram suitable for the discussion is shown in Figure 1. Two states *a* and *b* are assumed to exist for the system, with the system initially in the upper (or lower) excited state *a*, which may be a circular (high-*l*) Rydberg state. The transition to another (e.g. ground) state *b* is forbidden since angular momentum is not conserved for such a transition.[16] The system then oscillates between the states *a* and *b* with the frequency[17,18]

$$\Omega' \equiv (\Omega^2 + (\omega_L - \omega_E)^2)^{1/2} \tag{1}$$

where ω_L is the exciting (laser) angular frequency, and $\omega_E = \omega_{ab}$ is the corresponding quantity for the forbidden transition from *a* to *b* equal to $(E_a - E_b)/\hbar$. The sign of ω_E varies depending on the direction of ω_L, as shown in the three cases in Figure 1. Close to resonance with the transition downward as for a stimulated emission transition, the sign is as shown. For cases far from resonance that are discussed here, a negative sign is found for a case with nonallowed stimulated emission (case B in Figure 1). In the case similar to off-resonance absorption as in case A in Figure 1, the sign is changed such that $\omega_L + \omega_E$ enters the equation above. If the avoided transition is from the low state as in case C in Figure 1, the negative sign is retained. Ω is the Rabi frequency,

$$\Omega = \mathbf{D}_{ab} \cdot \mathbf{E}_0/\hbar \tag{2}$$

where $\mathbf{D}_{ab}$ is the transition moment between states *a* and *b*, and the electric field strength $\mathbf{E}_0$ is due to the radiation field. The transition moment $\mathbf{D}_{ab}$ between the excited state *a* and a low state *b*, like the ground state, is extremely small since it is strongly forbidden from the *l* selection rule and since the overlap between states *a* and *b* is very small. This also implies that Ω is small and thus that $\Omega' \approx \pm(\omega_L \pm \omega_E)$ is valid. It is practical to have $\Omega' > 0$, which means that

$$\Omega' = \omega_L \pm \omega_E \qquad \text{for } \omega_L > \omega_E$$

and

$$\Omega' = \omega_E \pm \omega_L \qquad \text{for } \omega_E > \omega_L$$

The first case is shown in Figure 1. The second case with the laser photon energy less than the energy of the forbidden transition is not discussed here. The time variation of the probability for transfer to the state *b* is[18]

$$c_b(t) \propto \sin \frac{\Omega' t}{2} \tag{3}$$

Since the transition from *a* to *b* is strongly forbidden, the system cannot transfer to the *b* state, but has to revert to the *a* state and emit the photon. This means that the process is a Rayleigh scattering process, but with an intrinsic delay. The time it takes for the system to go from the initial state *a* to the state *a* again is then found from

$$\frac{\Omega' t}{2} = \pi \tag{4}$$

This means that a delay

$$\tau = 2\pi/\Omega' = 2\pi/(\omega_L \pm \omega_E) = 1/c(\tilde{\nu}_L \pm \tilde{\nu}_E) \tag{5}$$

will be applied to the photon or light wave passing in and out through the highly excited state. The sign varies with the conditions of the avoided transition, as given in Figure 1. Since the system may oscillate for many such periods between the two states, multiples n of τ will also exist in the scattered light.

We will now study what happens with this type of multiply delayed scattered light when it is analyzed by a grating spectrometer. In general, the grating diffraction is given by the equation $m\lambda = |d \sin r - d \sin i|$, where i is the incoming angle toward the grating normal and r the similar outgoing angle, while m is the order of diffraction, λ the wavelength of the light, and d the grating groove spacing. In this case, the angles are taken with sign on each side of the grating normal. In the Czerny−Turner configuration used for the spectrometers, the condition for constructive interference becomes

$$m\lambda = 2d \cos\left(\frac{i_0 + r_0}{2}\right) \sin\theta \tag{6}$$

where θ is the angle of rotation in the spectrometer relative to the zero (specular) position, i_0 is the corresponding (design) incoming angle for the light with the grating in the $\theta = 0$ position, and r_0 is the corresponding outgoing angle (normally equal to i_0). If a delay $n\tau$ with n an integer also exists, the condition is instead

$$m\lambda = 2dC \sin\theta + n\tau c \tag{7}$$

with C a constant value due to the cosine factor and c the speed of light. The background for this equation is that for each groove in the grating an additional path difference exists due to the delay, such that the delay between each pair of grooves is τ. The delay along a small distance over the grating surface, say for N grooves, is then $N\tau$. As shown below, the number N is

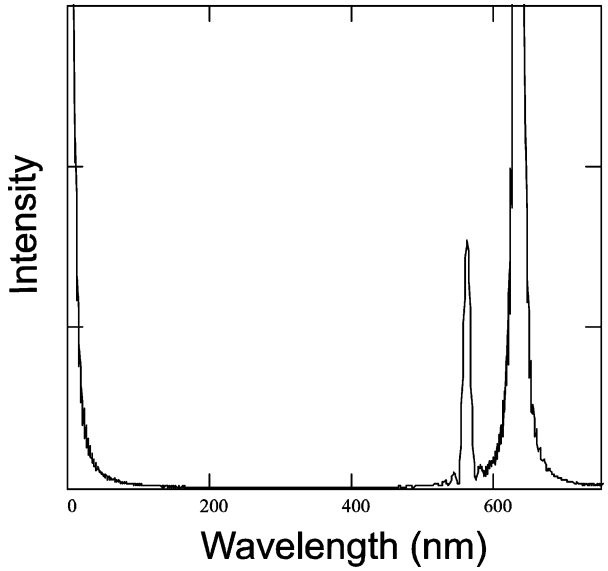

Figure 2. A calculated zero-order phase-delay band at 560 nm, as described in the theoretical section. The first-order laser line is at 632 nm, and the zero-order peak is to the left at 0 nm. The number of grooves involved on the grating is 50.

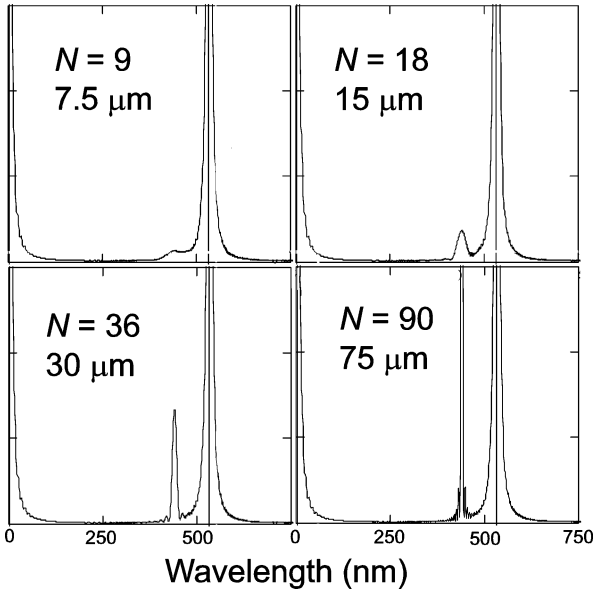

Figure 3. Calculated spectra as in Figure 2, but with a variable amount of the grating used for the formation of the band observed at 400 nm. The laser is at 532 nm. The number of lines N illuminated by the coherent phase-delayed light and the corresponding width of this illuminated area for a grating with a line density 1200 mm^{-1} are shown.

rather small, 10−50. Of course, also undelayed light exists at every groove, which will give a normal line for the laser light, as will also light with the same delay at adjacent grooves. Other combinations of delays could possibly give rise to higher order effects, but they will be much weaker and appear at larger angles from the main diffraction peak.

Two different cases have been identified, with $m = 0$ (zero-order flopping) and 1 (first-order flopping). For the zero-order case we describe the full signal dependence below, including the curve shape and peak width. The first-order case will be described elsewhere.

2.2. Zero-Order Flopping. The equation for diffraction from a grating[19] with a phase delay between adjacent grooves δ from the physical distance between the grooves describes ordinary diffraction. Adding also the phase difference due to a scattering delay $n\tau$ gives a final formula for the intensity[19]

$$I = N\frac{(\sin(N\delta/2))^2}{(\sin(\delta/2))^2} \tag{8}$$

The variable δ is found from

$$\delta = 2kdC\sin\theta + kn\tau c \tag{9}$$

where k is the wavenumber. The same principle is used in interferometric radio telescopes.[19] In the present case, most intensity will be averaged out due to interference, but the possibility of this process exists. It will give a diffraction pattern in this case.

It is possible to calculate the scattering as a function of the angle of the grating both for delayed and undelayed light. An example relevant to the present study is shown in Figure 2. The peak shown outside the laser peak is due to zero-order scattering with $\tau c = 560$ nm ($\tau = 1.9 \times 10^{-15}$ s) and with $N = 50$.

As will be described below, the peaks observed in the spectra are often rather broad. This means that the peaks may be formed by interaction with a small number of grooves $N = 10-50$ on the grating, as for the peak in Figure 2. The variation of the peak shape and intensity with N is shown in one example in Figure 3. The number of flopping cycles for which a coherent behavior exists has to be $\geq N$. This means as indicated in Figure 3 that the coherence is required to exist over only a small range of the grating surface, of the order of 0.1% of the total width of the grating, typically a distance of 50 μm. The Rabi-flopping cycle length τc is smaller than the wavelength of the light, and thus the flopping takes place for a period shorter than say 20 periods of the laser light. It is apparent that this type of flopping spectroscopy is most easily observed with gratings with a high line density, since this lessens the requirement of interference over a large area on the grating. This is confirmed in the experiments. It may also be expected that the flopping peaks will be more easily observed with an almost parallel beam to the monochromator slit, since the light will then fall on a relatively small spot of the grating. This should increase the visibility of the effect.

This description of consecutive phase shifts is the same as used to describe the phase shifting for linear arrays of radio telescope antennas.[19] The derivation gives finally

$$\tilde{\nu}_{obs} = \tilde{\nu}_L \pm \tilde{\nu}_E \tag{10}$$

for the cases shown in Figure 1, with the sign determined by the detailed process. This formula agrees in form with Stokes and anti-Stokes Raman scattering and is derived for zero-order diffraction, with $m = 0$ in eq 7.

This case is derived for a delay between consecutive lines on the grating of τ. This cannot of course be the only possibility, but diffraction from every second or every third line on the grating may also give a similar diffraction pattern. This means a smaller angle of deflection due to the delay, and for large nth diffraction, almost specular scattering should be observed. Following the derivation for this case, one finds that bands may be found around

$$\tilde{\nu}_{obs} = n(\tilde{\nu}_L \pm \tilde{\nu}_E) \approx n\tilde{\nu}_L \tag{11}$$

with $n = 2$ and 3 most commonly observed. These bands will probably be less well resolved than the bands around the laser line which have been described so far.

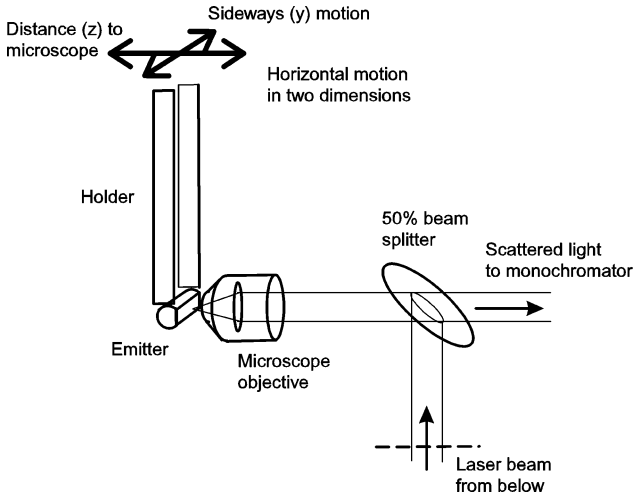

Figure 4. Experimental layout, with the two-dimensional motion of the emitter in front of the microscope indicated. The laser beam can be adjusted outside the figure by a roof prism adjustable in two dimensions, such that the beam entrance into the microscope is varied vertically and in the direction indicated as sideways (*y* motion).

3. Experimental Section

The experimental studies of Rydberg flopping use small He−Ne (632.8 nm) and Nd:YAG (532 nm) CW lasers with 2−30 mW power. The layout of the experiment is shown in Figure 4. The emitter can be moved in two dimensions by micrometers acting on the emitter holder, and the laser beam can be moved in two dimensions by micrometers acting on a roof prism that deflects the laser beam to the beam splitter. See further the figure caption. A Czerny−Turner monochromator is used for the experiments described in this study, an 0.5 m *f*/4 spectrometer (Spex 500M, ISA Inc.). The grating used has 1800 lines mm^{-1}. Another spectrometer at 0.32 m *f*/4.1 (Triax-320, ISA Inc.) has also been used with similar results, using other gratings. The spectrometers are run under computer control (SpectraMax 32, ISA Inc.).

The Rydberg species are formed by the type of solid-state Rydberg emitter (K doped catalyst) that is used in many other studies of Rydberg states.[1,6,8−10,20−24] It is an iron oxide material used on a large scale in industry for producing styrene from ethyl benzene[25] and is the same as type B used in a series of studies starting with ref 26. An Auger spectroscopy study[27] showed the surface concentration of K to be much higher than the specified initial bulk concentration of 6 atom %. High concentrations were also found for cleaved surfaces. Our preferred average value is 8 wt % of K. The emitter is normally mounted in a diffusion pumped vacuum chamber with a pressure of air of 1×10^{-4} mbar. A confocal setup is mainly used since it is then easily verified that the signal observed originates from the emitter by moving the emitter (in two dimensions) under the laser focus. (A large number of experiments has also been done without a microscope, with similar results and conclusions.) The microscope used is 40×, and the working distance to the emitter surface is approximately 0.4 mm. The diameter of the laser spot is approximately 10 μm. The monochromator is at a distance of 0.5 m from the emitter studied.

The question of grating ghosts and other similar artifacts should be treated briefly. The laser line intensity observed by the monochromator is relatively small. In the experiments, the total power reaching the monochromator slit is a few tens of a microwatt. Grating ghosts are normally reported in cases with intense light, and without such light reaching the grating as in the present study, it appears highly unlikely that such features should be observed. Further, holographic gratings, as used here, are free from ghosts. It is possible to adjust the setup such that only the scattered light from the sample enters the spectrometer. Stronger reflections from windows and other optical surfaces are not in the same direction. It is also observed in many cases that the scattered light giving the bands observed is not collinear with the main laser reflection from the surface as expected for stimulated Raman and similar processes, and the laser light can thus be prevented from entering the monochromator. Phase-delay spectra are observed also for such adjustments. Thus, it is concluded with certainty (after several years of experimentation) that the observed bands are not due to scattering ghosts or other similar artifacts.

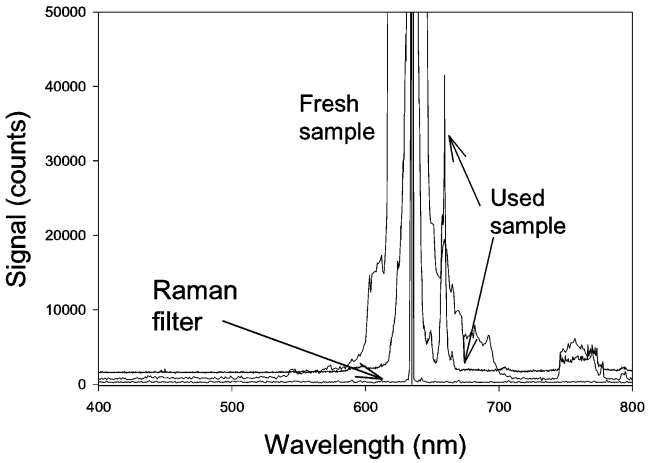

Figure 5. Typical phase-delayed spectra (30 mW He−Ne laser). The topmost spectrum is found for a fresh iron oxide catalyst sample. After some use in a vacuum, the sample is covered by carbon particles and hydrocarbon fragments, since the hydrocarbons from pump oils are catalytically dehydrogenated at the surface, giving the second spectrum (degassed surface at 1100 K). The Raman filter has a very high optical density at the laser line but transmits all light outside 632.8 ±5 nm. All features but the laser line are removed when this filter is used in front of the monochromator.

4. Results and Discussion

Phase-delay spectra with a large amount of information can be found. One example is shown in Figure 5, where typical spectra from a Rydberg emitter are shown. The top one is found for a new emitter, with high scattered intensity and broad bands. The middle curve is observed with a carbon-covered sample (due to hydrocarbon cracking) used for a long time in fore-vacuum pressure. It has a high peak at 653 nm due to hydrocarbon fragments on the surface. The grating band at 745−773 nm[23] is unchanged in this case.

A few predictions from the theory described above can be checked easily:

(1) The scattered light observed in the spectra should have the laser wavelength, not the wavelength indicated by the spectrometer.

(2) The scattered light in the spectra should not have the same linear polarization as the laser, since the delay will tend to produce elliptically polarized light.

(3) Bands should be observed at $n\tilde{\nu}_L$, n times the laser wavenumber.

Other points will also be treated below:

(4) If the signal observed is to be useful for spectroscopy, it must be formed at the sample surface.

(5) The signal formation in three different types of systems will be described in detail.

4.1. Scattered Laser Light. Various window and filter materials have been inserted in front of the spectrometer entrance slit and in front of the photomultiplier, behind the exit slit. In this way it is shown that the light giving the spectra does not have the wavelength indicated by the spectrometer. The spectral features are observed as long as the laser wavelength is not blocked, but blocking this wavelength removes all the features. This may be done for example by using a holographic Raman filter (a "Supernotch" filter with an optical density at the laser line of >4.0, Kaiser Optical Systems, Inc.) for the He−Ne laser wavelength. It rejects all light in the range 632.8 ± 5 nm. An example is shown in Figure 5, where the lowest curve is observed with the Raman filter. All bands including the grating band disappear, which means that they are all due to light of 632.8 nm wavelength or very close. Thus, the spectral information does not reach the detector as wavelength spectral information. The polarization state of the laser light has been varied in a controlled way, and the signal was not removed or changed in position on the wavelength scale. It is thus concluded that the spectra are formed from phase information in the laser light, as described by the theory given above.

4.2. Polarization Behavior. If the bands observed are due to phase-shifted laser light, other features showing phase shifts of the scattered light might be observed. The laser light is linearly polarized, and a phase shift of the scattered light might be observed also as a transformation to elliptically (or circularly) polarized light at the emitter. In principle, two possibilities exist to test for the existence of circularly polarized light from the emitter: (1) to scatter circularly polarized light and study the spectra observed relative to scattering of linearly polarized light and (2) to scatter linearly polarized light and test for circularly polarized light.

The first experiment is straightforward, using a quarter-wave plate to change the polarization state of the laser beam. Typical results are shown in Figure 6, where the circularly polarized light spectra are more intense than the spectra with linear polarized light, and a difference even exists between L and D polarized light. Both panels are from the same sweeps. Different bands change differently, which makes it unlikely that the changes are due to errors in alignment. Also, the Raman and plasma lines are constant in size, which shows that the laser intensity was constant. Thus, the emitter behaves in a different way for circularly relative to linearly polarized light.

The second experiment should in principle be even more conclusive, since the circularly polarized light should be directly observable. The setup tested blocks the linearly polarized light from the laser by a polarization filter (Polaroid) in front of the monochromator. Using a quarter-wave plate (at 45° to the linear direction of polarization) in front of this filter gives an increased signal as expected. However, we are unable to conclude that only circularly polarized light is observed.

4.3. Multiple Wavenumber Bands. The photomultipliers used have a shortwave sensitivity limit of around 190 nm. Measuring spectra over the maximum wavelength range as in Figures 6 and 7 reveals that intensity exists at wavelengths around 200 and 300 nm in the case of an exciting He−Ne laser. This light is easily shown to be red laser light. It is concluded that these bands are of the type described in eq 11.

4.4. The Surface Origin of the Signal. Tests can be done by moving the emitter sideways (*y* direction) as well as in the *z* direction (distance) relative to the microscope. By moving the emitter sideways with a focus on the surface, strong variations in the total scattered intensity can be observed at certain spots on the surface. The spectra also change in intensity,

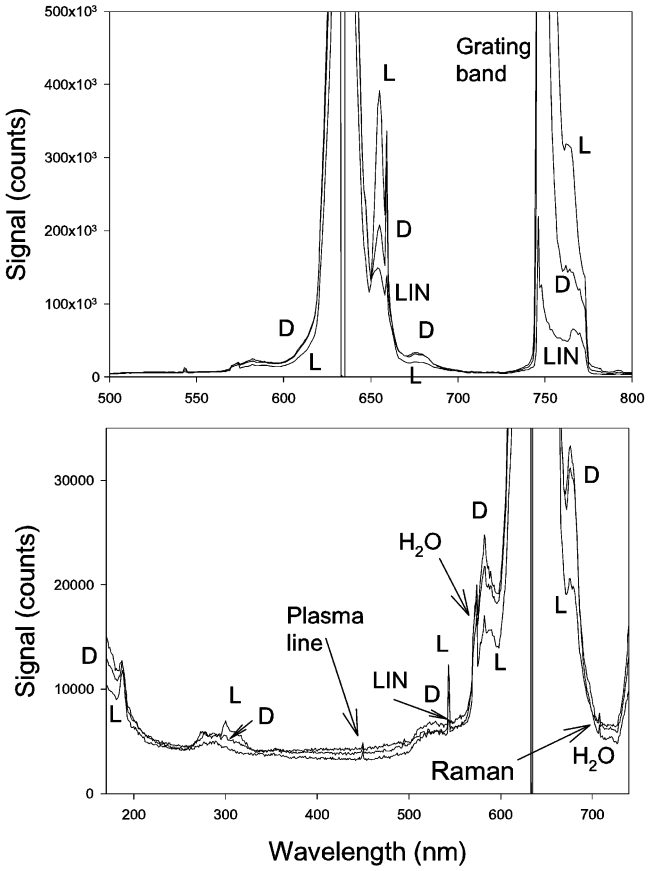

Figure 6. Effect of the polarization state of the laser (holographic grating 1800 mm^{-1}, water absorbed in a cold emitter, pressure 10^{-2} mbar, and 10 mW He−Ne laser). L and D indicate left and right circular polarization; the linear polarization is the third curve marked LIN. Observe the nontrivial ordering of the three consecutive spectra in different spectral ranges and for different bands.

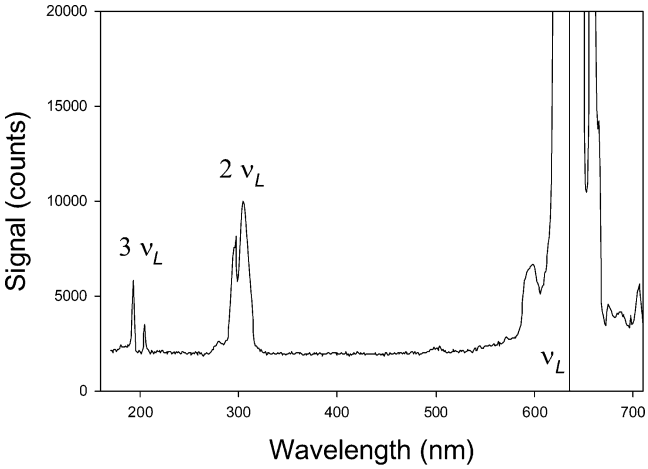

Figure 7. A phase-delay spectrum showing the weaker bands formed by interference between waves scattered from every second and every third line on the grating (large laser spot on sample, unfocused; 30 mW He−Ne laser; holographic grating 1800 mm^{-1}). See also Figure 6.

even in relative intensity of the peaks. Time variations are also observed, with a decrease in time for the most brilliant spots, which makes a systematic investigation rather difficult. Also during distance variation, spectra change in intensity and in relative intensity for different bands (peaks). In Figure 8, an experiment is done with a total change of distance to the microscope of 0.33 mm (see the figure for more details). The signal at the surface (0 μm) is maximum both for the phase-

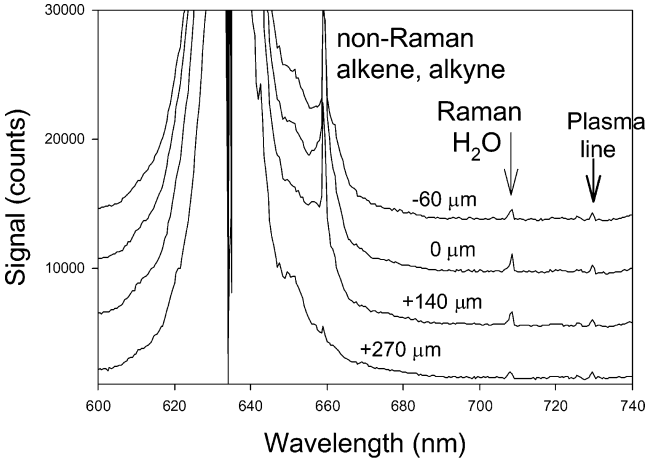

Figure 8. Proof of the surface origin of a phase-delay band due to hydrocarbon residues (grating 1800 mm^{-1}, cold emitter, 10^{-2} mbar of water vapor, 10 mW He−Ne laser). The distance between the emitter and the microscope is varied as indicated in the figure. Negative distance means that the focus is inside the emitter surface. Consecutive curves are shifted upward to increase visibility. Observe the different distance dependencies of the plasma line, the Raman band, and the non-Raman band.

delay band at 659 nm (shift 580 cm^{-1}) and for the Raman lines at larger shifts; however, the change with distance is much more rapid for the phase-delay band. The plasma line due to the laser at 728 nm does not vary at all, as expected. Thus, the surface sensitivity of the spectra is strong.

The same type of effect is also easily demonstrated by the experiment in Figure 9. The signal is measured both at a distance (de-focused spot on the emitter) from the surface and with focusing on the surface. The ratio of these two spectra is shown in the upper panel in the figure. Almost all scattered intensity around the laser line is unchanged, and thus not visible in the upper panel. Only the true added intensity from the surface is retained. A partial assignment is done as shown in the figure. It is clear that a spectrum is easily obtained from the surface of the emitter.

Another way to demonstrate the origin of the signal is to vary the temperature of the emitter. The experiment in Figure 10 shows two consecutively measured spectra, where the most intense spectrum is measured with a room temperature emitter. The low intensity spectrum was measured directly afterward, at high temperature (approximately 700 K). (An identical low-intensity, high-temperature spectrum was measured directly before the room temperature spectrum). The higher signal with the cold emitter is due to larger K density on the surface as seen directly from the size of the grating band. A partial assignment is given in the figure.

4.5. Processes of Signal Formation. The theoretical description used here assumes that the zero-order scattering depends on a highly excited Rydberg state, which itself gives spectra similar to anti-Stokes Raman scattering as shown in eq 10. It is then straightforward to assign peaks in the spectra to delay processes in Rydberg atoms such as K* atoms, where the state *a* is the Rydberg state and *b* the ground state. This has been done in refs 20 and 21 for K* Rydberg atoms and in Figure 10.

It is possible to observe phase-delay spectral bands for molecules also in the anti-Stokes range. An example is observed close to 500 nm in Figure 9. This band is assigned to a vibrational transition in H_2; thus the *a* state is thought to be K*-H_2(v=1) and the *b* state K*-H_2(v=0), following the form of case A in Figure 1. A transition $H_2(v=1) \rightarrow H_2(v=0)$ is forbidden since there is no permanent dipole moment in the

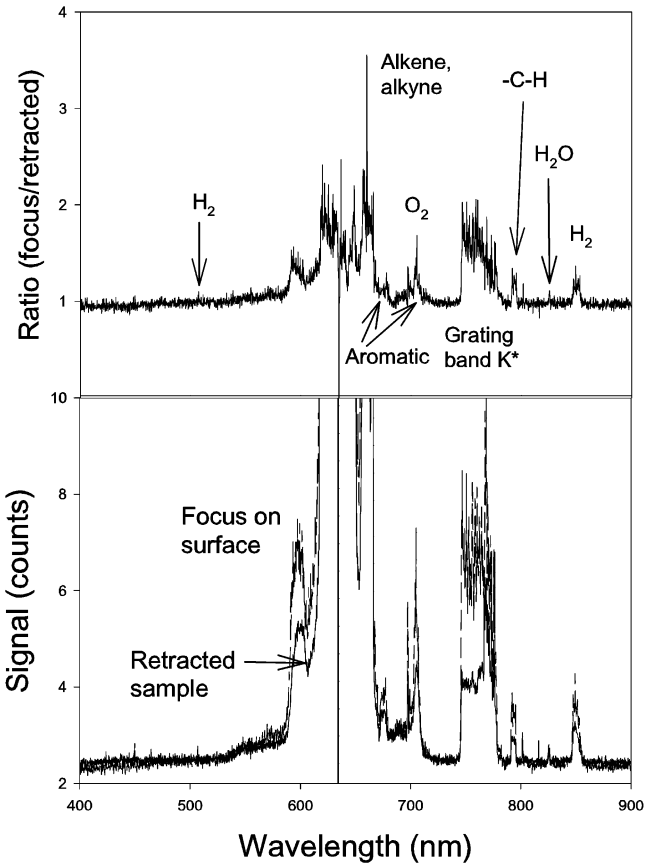

Figure 9. Comparison between one spectrum with focus on the surface and one spectrum unfocused (retracted from sample) (30 mW He−Ne laser; 10^{-4} mbar of air in chamber). The lower panel shows the focused spectrum (dashed) and the retracted one, while the upper panel shows the ratio between the two spectra. The features with higher intensity at focus stand out above the unity ratio.

hydrogen molecule, which means that the transition cannot take place. The role of K* is as an antenna, coupling the laser photons to the H_2 molecule. K* may also be responsible for the vibrational excitation of the H_2 molecule, transferring some energy from its electronic excitation.

However, most molecular bands described in the present study are in the Stokes range, at longer wavelengths than the laser. This means that case C in Figure 1 is applicable, where state *a* is lower than state *b* but still an excited Rydberg complex. This means that a flopping is performed between the *a* and *b* states, giving a process corresponding to case C in Figure 1. Thus, the sign is negative in eq 10 and the bands are observed in the Stokes range. Rydberg complexes of the type K*-H_2 are then responsible for the strong coupling to the laser light, while a real vibrational transition in H_2 is not very likely (but not strictly forbidden) since the molecule has no oscillating dipole moment due to the vibration. This means that the K* acts as an antenna in the process but otherwise only as a spectator. Many of the bands assigned may be of this type, but more complex processes have also been found.

One example of a more complex behavior is observed in the case of the K*-H_2O complex, which has been studied recently as reported elsewhere.[1] In the water molecule, all three vibrations are allowed both in IR and Raman. One Raman transition has been observed for this complex;[1] the two others may be very weak and will not interfer with the phase-delay process. The non-Raman band at 720 nm (1884 ± 50 cm^{-1}) has been studied in detail.[1] The *a* state in this case seems to be the (K-OH_2(v=0))* and the *b* state the corresponding v = 1 state,

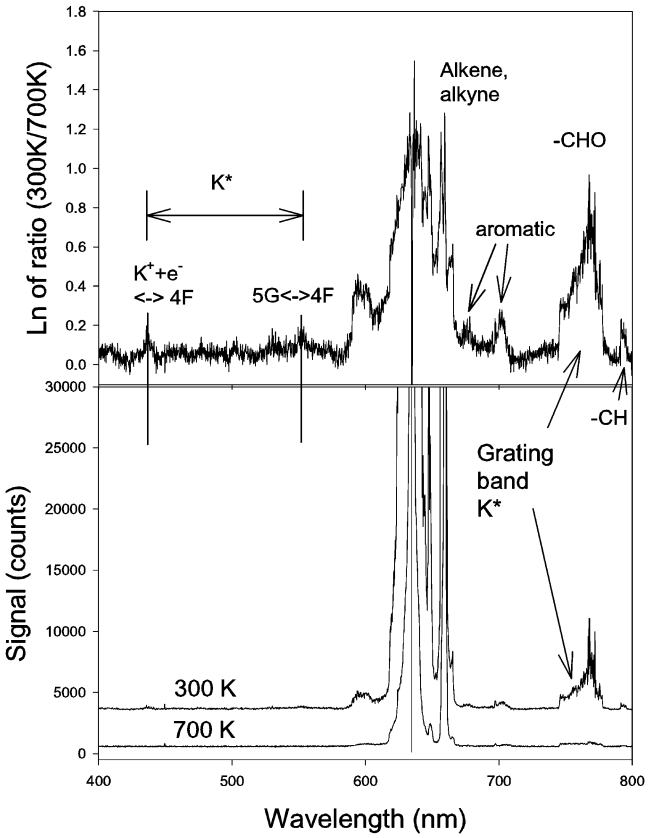

Figure 10. The effect of temperature changes (10^{-4} mbar of air in chamber). The lower panel shows a cold spectrum at the top (displaced upward) and a spectrum from the hot sample (700 K) at the bottom. In the upper panel, the log of the ratio between the two spectra is displayed. The region indicated K* is where apparent transitions in K Rydberg species are observed.

thus with the *b* state higher. This corresponds to case C in Figure 1. The observed band position agrees well with the energy difference between the two lowest vibrational states in the electronically excited H_2O^* $\tilde{A}(^1B_1)$ (and with another transition in the H_2O^* $\tilde{B}(^1A_1)$ state[28]). The fact that all electronically excited states of H_2O are Rydberg states probably means that a Rydberg complex $(K\text{-}OH_2)^*$ is formed preferentially instead of just leading to vibrational excitation as might happen in the H_2 case described above. The sign becomes negative in eq 10, which brings the band to smaller wavenumbers than the laser, thus into the Stokes range. From the results observed, it seems that the Raman process is here of lower probability than the phase-delay process.

A process that gives a behavior resembling the observed spectra is the fluorescence process giving rise to the so-called Mollow triplet.[29] It gives rise to symmetrically placed sidebands around the driving laser frequency, at the distance $\pm\Omega$, i.e., with real frequency shifts. Such shifts would not be observable in the present setup due to the small shifts expected even for atomic systems;[30,31] the value of Ω is also much smaller in the present case, which would give very small shifts. Further, the bands observed here are formed by the exciting laser photons with no frequency shift.

From the results presented here, in Figures 9 and 10, and especially from ref 1 it is apparent that molecular information can be found by the phase-delay method. The band position may be slightly different from that in a Raman process, however, since the K* coupling to the molecule will influence the molecular levels slightly. However, in Figures 9 and 10, the agreement is good.

5. Conclusions

It is shown that Raman-like spectra can be obtained from the surface boundary layers at emitters forming Rydberg states. The spectra show bands in both the Stokes and the anti-Stokes ranges. The origin from the solid emitter surface is proved by the use of a microscope setup, with focusing to a diameter of 10 μm. The spectra are observed by grating spectrometers, but the light from the exciting laser is scattered with no spectral shift. A theory of phase-delayed light is developed that describes the formation of the spectra. The spectra have already proved useful for the study of adsorbed species such as K and H_2O on catalyst surfaces.

Acknowledgment. The author thanks P. Govind Menon from whom the catalyst samples were obtained and S. Wall from which the laser used in most measurements was borrowed. Discussions with Shahriar Badiei are gratefully acknowledged.

References and Notes

(1) Olofson, F.; Badiei, S.; Holmlid, L. *Langmuir* **2003**, *19*, 5756.
(2) Engvall, K.; Kotarba, A.; Holmlid, L. *Catal. Lett.* **1994**, *26*, 101.
(3) Kotarba, A.; Dmytrzyk, J.; Narkiewicz, U.; Baranski, A. *React. Kinet. Catal. Lett.* **2001**, *74*, 143.
(4) Kotarba, A.; Adamski, G.; Sojka, Z.; Witkowski, S.; Djega-Mariadassou, G. *Stud. Surf. Sci. Catal.* **2000**, *130A*, 485.
(5) Kotarba A.; Baranski, A.; Hodorowicz, S.; Sokolowski, J.; Szytula, A.; Holmlid, L. *Catal. Lett.* **2000**, *67*, 129.
(6) Kotarba, A.; Engvall, K.; Pettersson, J. B. C.; Svanberg, M.; Holmlid, L. *Surf. Sci.* **1995,** *342*, 327.
(7) Wang, J.; Engvall, K.; Holmlid, L. *J. Chem. Phys.* **1999**, *110*, 1212
(8) Holmlid, L.; Menon, P. G. *Appl. Catal. A* **2001**, *212*, 247.
(9) Badiei, S.; Holmlid, L. *Chem. Phys. Lett.* **2003**, *376*, 812.
(10) Holmlid, L. *J. Phys. B*: *At. Mol. Opt. Phys.* **2004**, *37*, 357.
(11) Ayars, E. J.; Hallen, H. D. *Phys. Rev. Lett.* **2000**, *85*, 4180.
(12) Haslett, T. L.; Tay, L.; Moskovits, M. *J. Chem. Phys.* **2000**, *113*, 1641.
(13) Fleischmann, M.; Hendra, P. J.; McQuilla, A. J. *Chem. Phys. Lett.* **1974**, *26*, 163.
(14) Kneipp, K.; Wang, Y.; Kneipp, H.; Perelman, L. T.; Itzkan, I.; Dasari, R.; Feld, M. S. *Phys. Rev. Lett.* **1997**, *78*, 1667.
(15) Nie, S.; Emory, S. R. *Science* **1997**, *275*, 1102.
(16) Gallagher, T. F. *Rydberg Atoms*; Cambridge University Press: Cambridge, UK, 1994.
(17) Metcalf, H.; van der Straten, P. *Laser Cooling and Trapping*; Springer: New York, 1999.
(18) Demtröder, W. *Laser Spectroscopy, Basic Concepts and Instrumentation*, 2nd ed.; Springer: Berlin, Germany, 1996.
(19) Hecht, E. *Optics*, 3rd ed.; Addison-Wesley: Reading, MA, 1998.
(20) Holmlid, L. *Langmuir* **2001**, *17*, 268.
(21) Holmlid, L. *Astrophys. J.* **2001**, *548*, L249.
(22) Engvall, K.; Kotarba, A.; Holmlid, L. *J. Catal.* **1999**, *181*, 256.
(23) Holmlid, L. *J. Opt. Soc. Am. A* **2001**, *18*, 367.
(24) Badiei, S.; Holmlid, L. *Chem. Phys.* **2002**, *282*, 137.
(25) Meima, G.; Menon, P. G. *Appl. Catal. A* **2001**, *212*, 239.
(26) Engvall, K.; Holmlid, L.; Menon, P. G. *Appl. Catal.* **1991**, *77*, 235.
(27) Lundin, J.; Holmlid, L.; Menon, P. G.; Nyborg, L. *Ind. Eng. Chem. Res.* **1993**, *32*, 2500.
(28) Wang, H.-t.; Felps, W. S.; McGlynn, S. P. *J. Chem. Phys.* **1977**, *67*, 2614.
(29) Mollow, B. R. *Phys. Rev.* **1969**, *188*, 1969.
(30) Hartig, W.; Walther, H. *Appl. Phys.* **1973**, *1*, 171.
(31) Grove, R. E.; Wu, F. Y.; Ezekiel, S. *Phys. Rev. A* **1977**, *15*, 227.